Article

Harnessing intestinal tryptophan catabolism to relieve atherosclerosis in mice

Mouna Chajadine[1], Ludivine Laurans[1,10], Tobias Radecke[1,10], Nirmala Mouttoulingam[1], Rida Al-Rifai [1], Emilie Bacquer[1], Clara Delaroque[2,3], Héloïse Rytter[2,3], Marius Bredon[4,5], Camille Knosp[1], José Vilar [1], Coralie Fontaine[6], Nadine Suffee [1], Marie Vandestienne [1], Bruno Esposito[1], Julien Dairou[7], Jean Marie Launay[8], Jacques Callebert[8], Alain Tedgui [1], Hafid Ait-Oufella [1], Harry Sokol [4,5,9], Benoit Chassaing [2,3] & Soraya Taleb [1] ✉

Tryptophan (Trp) is an essential amino acid, whose metabolism is a key gatekeeper of intestinal homeostasis. Yet, its systemic effects, particularly on atherosclerosis, remain unknown. Here we show that high-fat diet (HFD) increases the activity of intestinal indoleamine 2, 3-dioxygenase 1 (IDO), which shifts Trp metabolism from the production of microbiota-derived indole metabolites towards kynurenine production. Under HFD, the specific deletion of IDO in intestinal epithelial cells leads to intestinal inflammation, impaired intestinal barrier, augmented lesional T lymphocytes and atherosclerosis. This is associated with an increase in serotonin production and a decrease in indole metabolites, thus hijacking Trp for the serotonin pathway. Inhibition of intestinal serotonin production or supplementation with indole derivatives alleviates plaque inflammation and atherosclerosis. In summary, we uncover a pivotal role of intestinal IDO in the fine-tuning of Trp metabolism with systemic effects on atherosclerosis, paving the way for new therapeutic strategies to relieve gut-associated inflammatory diseases.

The gastrointestinal tract has become recognized as a central organ in linking diet and cardiovascular diseases (CVDs), including atherosclerosis[1]. Particularly, the gut microbiota has been identified as a potential mediator that could impact atherosclerosis[2]. Although experimental and clinical data point to a critical role of intestinal inflammation in increased risk of CVD, little is known about the mechanisms whereby the intestine might specifically contribute to atherosclerosis. Particularly, diet-induced disruption of gut homeostasis might cause systemic deleterious conditions leading to atherosclerosis.

Tryptophan (Trp) is one of the essential amino acids provided by the diet, whose metabolism appears as a key metabolic gatekeeper of

[1]Université Paris Cité, Inserm, PARCC, F-75015 Paris, France. [2]Microbiome-Host interactions, Institut Pasteur, Université Paris Cité, INSERM U1306, Paris, France. [3]INSERM U1016, Team "Mucosal microbiota in chronic inflammatory diseases", CNRS UMR10 8104, Université Paris Cité, Paris, France. [4]Sorbonne Université, INSERM, Centre de Recherche Saint-Antoine, CRSA, AP-HP, Saint Antoine Hospital, Gastroenterology Department, F-75012 Paris, France. [5]Paris Centre for Microbiome Medicine (PaCeMM) FHU, Paris, France. [6]Inserm U1297, Institut des Maladies Métaboliques et Cardiovasculaires, Université de Toulouse, BP 84225, 31 432 Toulouse cedex 04, cedex, France. [7]Université Paris cité, CNRS, Laboratoire de Chimie et de Biochimie Pharmacologiques et Toxicologiques, F-75006 Paris, France. 45 rue des Saints Pères, 75006 Paris, France. [8]Assistance Publique Hôpitaux de Paris, Service de Biochimie and INSERM U942, Hôpital Lariboisière, Paris, France. [9]Université Paris-Saclay, INRAe, AgroParisTech, Micalis institute, Jouy-en-Josas, France Université Paris-Saclay, INRAe, AgroParisTech, Micalis institute, Jouy-en-Josas, France. [10]These authors contributed equally: Ludivine Laurans, Tobias Radecke. ✉e-mail: soraya.taleb@inserm.fr

intestinal homeostasis. Trp is involved in various physiological processes and contributes to the maintenance of intestinal and systemic homeostasis in health and disease[3–5]. In mice, dietary lack of Trp leads to impaired intestinal immunity and gut microbiota dysbiosis, which causes intestinal inflammation and diarrhea[6]. In humans, patients with inflammatory bowel disease (IBD) exhibit disturbed tryptophan metabolism on both host and microbiota sides[7,8]. However, despite the importance of intestinal Trp metabolism in gut homeostasis along with the ascertainment that intestinal inflammation is associated with CVDs, the systemic impact of impaired gut Trp metabolism on atherosclerosis is still unclear.

Under homeostatic conditions, intestinal Trp catabolism follows three pathways[9], which consist in the Kynurenine (Kyn) pathway, mainly acting in intestinal epithelial cells (IECs) via the enzyme indoleamine 2, 3-dioxygenase 1, IDO (~95% of Trp); the gut microbiota pathway of direct transformation of Trp into indole metabolites (~5% of Trp); and the serotonin or 5-hydroxytryptamine (5-HT) pathway in enterochromaffin cells (ECs) via Trp hydroxylase 1 (TPH1) (~1-2% of Trp), which accounts for the majority (~90%) of whole body 5-HT production.

Previous studies reported either proatherogenic[10,11] or atheroprotective effects[12] of IDO. In particular, prior work by our group has shown that the global invalidation of IDO dampened atherosclerosis under high-cholesterol diet (HCD) feeding[12]. This proatherogenic effect was attributed to increased IDO expression in myeloid cells, involving the Kyn pathway, especially kynurenic acid[12]. In a subsequent study, we revealed a critical role for IDO in the fine-tuning of intestinal Trp metabolism under conditions of obesogenic high-fat diet (HFD), with major consequences on metabolic syndrome[13]. However, the specific role of intestinal IDO in cardiometabolic diseases, including atherosclerosis, is still unknown. Moreover, although recent studies highlighted the local effects of Trp-derived metabolites in intestinal homeostasis[9], their systemic impacts on atherosclerosis is poorly known. In this work, we demonstrate that HFD increases intestinal IDO activity, while decreasing the production of indole metabolites. Functional studies of Trp catabolic pathways reveal a protective role of intestinal IDO and indole metabolites, in contrast to the detrimental role of serotonin in atherosclerosis.

Results
HFD has a major effect on intestinal Trp catabolism in a mouse model of atherosclerosis
First, we assessed the effect of diet on intestinal Trp catabolic pathways (Kyn, 5-HT and indole pathways) using low-density lipoprotein receptor-deficient ($Ldlr^{-/-}$) mice, as a validated model of atherosclerosis. In particular, we examined the effect of HCD, a proatherogenic diet, as well as the effect of HFD, which has previously been shown to increase intestinal IDO activity in C57Bl/6 mice[13]. For this purpose, $Ldlr^{-/-}$ mice were fed with either a normal chow diet (NCD) and the purified diets HFD, HCD, or the combination of HFD + HCD for 13 weeks (Supp. Figure 1A). As shown in Fig. 1A, intestinal Trp levels decrease along with a marked increase in Kyn levels, indicating a substantial increase in intestinal IDO activity (as assessed by Kyn/Trp ratio), under HFD conditions (HFD or HFD + HCD) compared to NCD or HCD (Fig. 1A). In agreement with previous reports[13,14], indole levels decreased under HFD conditions (with or without HCD) compared to HCD alone (Fig. 1B). Intestinal 5-HT levels also decreased in HFD conditions (HFD or HFD + HCD) compared to NCD or HCD (Fig. 1C). These data indicate that HFD, but not HCD, had a major effect on intestinal Trp metabolism through promoting the Kyn pathway to the detriment of the pathways of indole and 5-HT.

Next, we investigated the mechanisms underlying the observed increase in intestinal IDO activity under HFD. Short-chain fatty acids (SCFAs), such as acetate and butyrate, are the end products of the fermentation of dietary fibers by the anaerobic intestinal microbiota[15]. Recently, it was shown that butyrate, one of the SCFAs, negatively regulated IDO expression in IECs[16], suggesting a potential role of dietary fibers-induced bacterial SCFA metabolites in the regulation of Trp metabolism. In agreement with previous reports[17], mice fed HFD (containing a low level of fibers)[18] but not HCD, exhibited a decrease in acetate and butyrate levels in feces (Supp. Figure 1B). Interestingly, the supplementation with soluble fibers like FOS (fructo-oligosaccharids) to $Ldlr^{-/-}$ mice fed HFD increased SCFA production, including acetate and butyrate (Supp. Figure 1C), and led to a significant decrease in fecal Kyn levels without significant differences in fecal Trp levels (Fig. 1D and Supp. Figure 1D), further suggesting the importance of fibers-mediated SCFA production in the regulation of the intestinal IDO activity. Taken together, these data indicate that feeding mice with HFD, which contains low levels of fibers, led to reduced SCFA production, including butyrate, a negative regulator of IEC IDO[16], which could explain, at least in part, the observed increase in intestinal IDO activity under this condition.

IDO expressed in IECs has a protective role in atherosclerosis under HFD
We next explored the role of intestinal IDO in atherosclerosis. For this purpose, mice devoid of IDO in IECs ($Ido-1^{flox/flox}$ villin-cre) were generated by crossing loxP-flanked $Ido-1$ mice ($Ido-1^{flox/flox}$) with mice expressing Cre recombinase under the control of the murine villin promoter (villin-cre + /−). Then, we crossed $Ido-1^{flox/flox}$ Villin-cre (IEC IDOKO) mice with $Ldlr^{-/-}$ mice. Male $Ldlr^{-/-}$ IEC IDOKO and littermate control mice ($Ldlr^{-/-}$ IEC IDO) were fed for 8 weeks with either NCD or HFD combined with HCD (HFD + HCD) to induce intestinal IDO activity and atherosclerosis, respectively. The absence of IDO in IECs led to a substantial decrease in $Ido-1$ mRNA expression in small intestines compared to controls (Supp. Figure 1E) despite increased $Ido-1$ mRNA in the small intestine FACS-sorted CD45+ cells (Supp. Figure 1F), underscoring the importance of IDO expression in IECs in intestinal Trp metabolism. Moreover, as shown above, $Ldlr^{-/-}$ IEC IDO mice fed HFD + HCD had increased intestinal IDO activity (as assessed by Kyn/Trp ratio) compared to $Ldlr^{-/-}$ IEC IDO mice fed NCD (Fig. 1E). In addition, IDO activity (Kyn/Trp) in small intestines was dampened in absence of IDO in IECs (Fig. 1E). This was also true in blood, as shown by increased plasma Kyn/Trp ratio in HFD + HCD compared to NCD, and marked decrease in plasma Kyn/Trp ratio in $Ldlr^{-/-}$ IEC IDOKO mice fed HFD + HCD at a level similar as in $Ldlr^{-}$ IEC IDOKO mice fed NCD (Fig. 1F), emphasizing the prominence of IEC IDO activity under HFD to the systemic Trp metabolism. Of note, Kyn/Trp ratio was much higher in the small intestines than in the colons (Supp. Figure 1G), indicating the importance of the small intestine in the Kyn pathway. Remarkably, male $Ldlr^{-/-}$ IEC IDOKO mice fed HFD + HCD exhibited an increase in plaque size in the aortic sinus compared to the littermate $Ldlr^{-/-}$ IEC IDO mice fed HFD + HCD without any changes in plasma cholesterol levels (Fig. 1G, H), indicating that IEC IDO exerts a protective role against atherosclerosis under HFD.

Then, we sought to know whether this protective effect prevailed over a longer period of HFD + HCD feeding, in advanced atherosclerosis. Thus, male $Ldlr^{-}$ IEC IDOKO mice and their littermate controls were fed HFD + HCD for 13 weeks. As shown in Supp. Figure 2A-D, no major differences in mouse body weight, and metabolic parameters including insulin tolerance test (ITT), oral glucose tolerance test (OGTT), and insulin-resistance index (HOMA-IR) were observed between the two groups. Moreover, we found no significant differences in plasma cholesterol and plaque size (in the aortic sinus) between the two groups of mice, after 13 weeks of HFD + HCD (Supp. Figure 2E and F). The absence of effects after a long period of HFD + HCD feeding in males was likely due to the significant decrease in $Ido-1$ gene expression in the small intestines of control mice at 13 weeks compared to 8 weeks (Supp. Figure 2G).
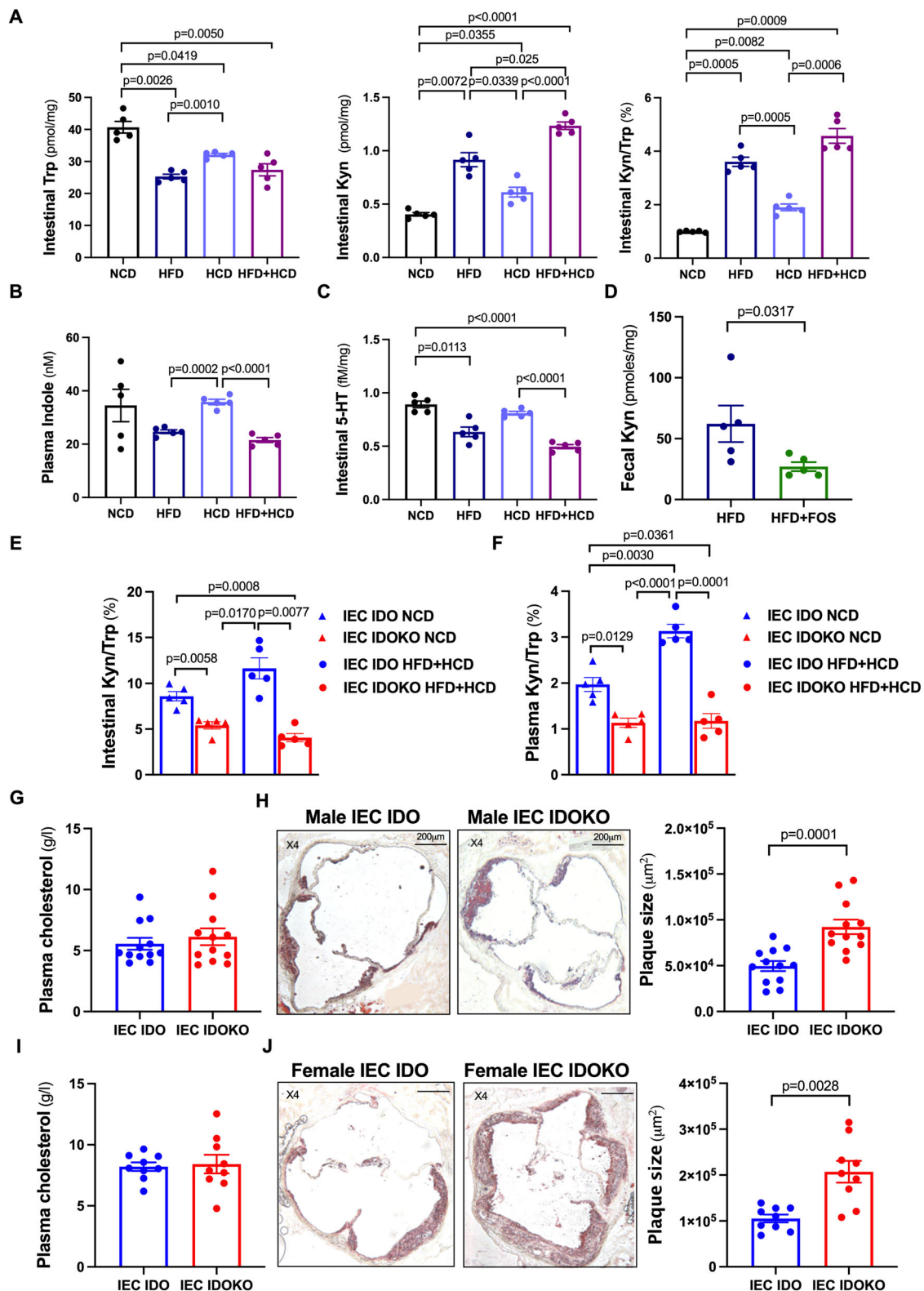
Then, we examined plaque size in females at short (8 weeks) and long period (13 weeks) of HFD + HCD. At 8 weeks of HFD + HCD, the absence of IDO in IECs did not significantly impact plaque size (in the aortic sinus) and plasma cholesterol levels, despite a significant decrease in *Ido-1 mRNA* in the small intestines (Supp. Figure 3A-C). We then analyzed atherosclerotic plaques after 13 weeks of HFD + HCD. Remarkably, female mice with IDO deletion in IECs had increased plaque size in the aortic sinus without significant changes in plasma

cholesterol levels (Fig. 1I-J). The increase in plaque size was also observed in the thoracic aorta (Supp. Figure 3D). Interestingly, *Ido-1* mRNA was markedly increased in female control mice at 13 weeks compared to 8 weeks of HFD + HCD feeding (Supp. Figure 3E). Moreover, *Ido-1 mRNA* was higher in the intestine of female compared to male control mice after 13 weeks of HFD + HCD (Supp. Figure 3F), which most likely explain why the impact of intestinal IDO on plaque size in female mice was observed in advanced but not in early

Fig. 1 | Induction of IEC IDO by HFD has a protective role in atherosclerosis.
A Tryptophan (Trp), Kynurenine (Kyn) levels, and related Kyn/Trp ratio (%) in the small intestine extracts ($n = 5$ mice/group), **B** plasma indole levels in the portal vein, **C**. 5-hydroxytryptamine (5-HT) in the small intestine extracts of male $Ldlr^{-/-}$ mice fed either normal chow diet (NCD), high-fat diet (HFD), or high-cholesterol diet (HCD) or the combination of both HFD + HCD for 13 weeks ($n = 5$ mice/group). **D** Kyn levels in feces of $Ldlr^{-/-}$ mice fed HFD supplemented or not with FOS for 13 weeks ($n = 5$ mice/group). **E, F** Kyn/Trp ratio (%) in the small intestine extracts and plasma in male $Ldlr^{-/-}$ IEC IDO KO and littermate control $Ldlr^{-/-}$ IEC IDO mice ($n = 5$ mice/group), after 8 weeks of HFD + HCD or NCD feeding period. NCD

represents the control group without atherosclerosis development. **G.** Plasma cholesterol, **H** representative pictures, and quantifications of plaque size in the aortic sinus in male $Ldlr^{-/-}$ IEC IDO KO ($n = 12$ mice) and littermate control $Ldlr^{-/-}$ IEC IDO ($n = 12$ mice) fed HFD + HCD for 8 weeks; scale bar 200 μm. **I** Plasma cholesterol, **J** representative pictures and quantifications of plaque size in the aortic sinus in female $Ldlr^{-/-}$ IEC IDO KO ($n = 9$ mice), and littermate controls $Ldlr^{-/-}$ IEC IDO ($n = 9$ mice) fed HFD + HCD for 13 weeks; scale bar 200 μm. Individual data are presented as scattered dot plots, with the mean and s.e.m. The p values were determined using the Brown-Forsythe one-way ANOVA test followed by Tukey's multiple comparison test. Source data are provided as a Source Data file.

atherosclerosis. Of note, a decrease in gene expression of estrogen receptors (*esr1* and *esr2 mRNA*), as well as that of their target gene *greb1*[19], was observed in the small intestines of females. On the contrary, increased expression of these genes were found in males after 13 weeks of HFD + HCD (Supp. Figure 3G-H). Moreover, an inverse correlation between *Ido-1 mRNA* and *esr2 mRNA* was observed in the small intestines of both males and females after 13 weeks of HFD + HCD (Supp. Figure 3I), suggesting a differential sex hormone regulation of IDO expression within the gut.

In agreement with a major effect of HFD in inducing intestinal IDO activity, both male and female IEC IDO KO mice fed with only HCD did not display any significant differences in plaque size in the aortic sinus and plasma cholesterol levels despite a marked decrease in *Ido-1 mRNA* in IEC IDOKO (Supp. Figure 4), further pointing to the importance of HFD in intestinal IDO-mediated effects on atherosclerosis.

Taken together, these findings demonstrate that under HFD condition, IDO expressed in IECs protects against atherosclerosis in both males and females, in a sex- and time-dependent manner.

Intestinal IDO decreases local and systemic inflammation

Then, we sought to assess the mechanisms that could account for the pro-atherogenic effects of intestinal IDO deficiency. Gut inflammation is known to be associated with increased susceptibility to CVD[1]. This may be due to alterations of the intestinal barrier, leading to enhanced permeability and translocation of microbial molecules, such as lipopolysaccharides (LPS), to the bloodstream, resulting in sustained peripheral inflammatory responses[20]. Interestingly, after 8 weeks of HFD + HCD feeding, male $Ldlr^{-/-}$ IEC IDO KO mice displayed a range of features of intestinal inflammation, including elevated levels of fecal lipocalin-2 (Lcn2), a sensitive marker for gut inflammation[21], as well as increased pathohistological scores of colonic sections, compared to littermate controls (Fig. 2A, B). In agreement with this observation, we detected a decrease in the average distance between the closest bacteria and the epithelium surface in intestinal IDO-deficient mice (Fig. 2C) indicative of microbiota encroachment known to be associated with chronic intestinal inflammation[22]. Moreover, this was associated with increased intestinal expression of inflammatory factors such as tumor necrosis factor (TNF)α and interferon (IFN)γ as well as the chemokine and chemokine receptors-encoding genes XCL1, CXCR6, and CCR10 (Supp. Figure 5A-B). Also, flow cytometry analysis of the small intestine lamina propria showed higher numbers of T lymphocytes including CD4$^+$ and CD8$^+$ cells (Fig. 2D and Supp. Fig. 6A), without significant changes in T helper (Th) polarization (expressed as % of CD4): no differences in Th1-specific T box transcription factor (T-bet), Th17-specific RAR-related orphan receptor (ROR)-γt, or T regulatory cells (Treg)-specific forkhead box P3 (Foxp3) expression (Supp. Fig. 6B-C). In addition, we found decreased expression of the tight junction occludin-1 gene (Supp. Fig. 6D), as well as elevated levels of serum IgG antibodies to LPS (Fig. 2E), suggesting increased intestinal permeability. Consistently, female $Ldlr^{-/-}$ IEC IDOKO mice fed HFD + HCD for 13 weeks displayed increased colon pathohistological scoring (Supp. Fig. 7A), as well as serum FITC-dextran 4000 Da levels following oral gavage (Fig. 2F), compared to controls, providing further evidence for increased intestinal permeability in the absence of intestinal IDO.

Moreover, blood lymphocyte numbers, including CD4 + , CD8 + , and B lymphocyte CD19+ cells, were increased in male IEC IDOKO mice, as assessed by flow cytometry analysis (Supp. Fig. 7B).

Collectively, these data suggest an increase in gut inflammation and alteration in the intestinal barrier in the absence of intestinal IDO, which may cause systemic inflammation.

Then, we wanted to examine systemic inflammation, particularly within the atherosclerotic plaques. Analysis of plaques in male $Ldlr^{-/-}$ IEC IDOKO mice after 8 weeks of HFD + HCD revealed marked proinflammatory phenotype, as assessed by increased accumulation of CD3$^+$ T cells (Fig. 2G) and large necrotic cores (Supp. Fig. 7C), compared to control mice. The increase in necrotic core size was also observed in female $Ldlr^{-/-}$ IEC IDOKO mice after 13 weeks of HFD + HCD (Supp. Fig. 7D). No differences in MOMA2$^+$ macrophages were observed between the 2 groups in male mice (Supp. Fig. 7E).

To further evaluate whether increased T cells, known to promote atherosclerosis[23], was involved in the pro-atherogenic phenotype observed in IEC IDOKO mice, we generated a mouse model of atherosclerosis deficient for both intestinal IDO and lymphocytes ($Ldlr^{-/-}Rag_1^{-/-}$ IEC IDOKO mice) and compared them to $Ldlr^{-/-}Rag_1^{-/-}$ IEC IDO littermate mice. As shown in Fig. 2H, I, lymphocyte deficiency abrogated the pro-atherogenic effects observed in the absence of intestinal IDO without significant changes in plasma cholesterol levels, suggesting a major role for lymphocytes in this process. Taken together our data indicate that the absence of intestinal IDO promotes gut and plaque inflammation.

Intestinal 5-HT exerts a pro-atherogenic role

IDO is known to catabolize Trp into Kyn, which is the common metabolite upstream of the Kyn-derived metabolites. First, we sought to examine whether a decrease in Kyn levels observed in $Ldlr^{-/-}$ IEC IDO KO was responsible for the observed phenotype. For this purpose, we supplemented $Ldlr^{-/-}$ IEC IDO KO mice with Kyn (Supp. Fig. 8A) during the 8 weeks of HFD + HCD feeding. As shown in Supp. Fig. 8B, there was no correlation between fecal Kyn levels and plaque size, suggesting that the main pathway responsible for the observed phenotype was unlikely dependent on Kyn or Kyn-derived metabolites.

We then investigated the other Trp-dependent pathways, particularly 5-HT, which was previously shown to exert a deleterious role in several inflammatory diseases such as myocardial infarction[24] and colitis[25]. Intestinal 5-HT levels were not significantly changed in control mice fed 8 weeks of HFD + HCD, compared to mice fed NCD (Supp. Fig. 8C). To examine whether intestinal 5-HT was involved in atherosclerosis, we specifically inhibited TPH1, which is responsible for 5-HT production within the gut (~ 90% of total serotonin[26]). $Ldlr^{-/-}$ mice fed HFD + HCD for 8 weeks treated with TPH1 inhibitor (LP533401) exhibited a marked decrease in 5-HT production in the small intestine (Fig. 3A), as well as in the blood (Supp. Fig. 8D). The inhibition of TPH1 was associated with an increase in indole production, as assessed by a higher fecal IAA and indole production, without any significant changes in IDO activity in the small intestine and plasma, as assessed by Kyn/Trp ratio (Supp. Fig. 8E-G). This was accompanied by an enhanced intestinal expression of anti-microbial peptides, regenerating islet-derived (Reg)3 g, Reg3b as well as occludin-1 genes (Supp. Fig. 8H-I).
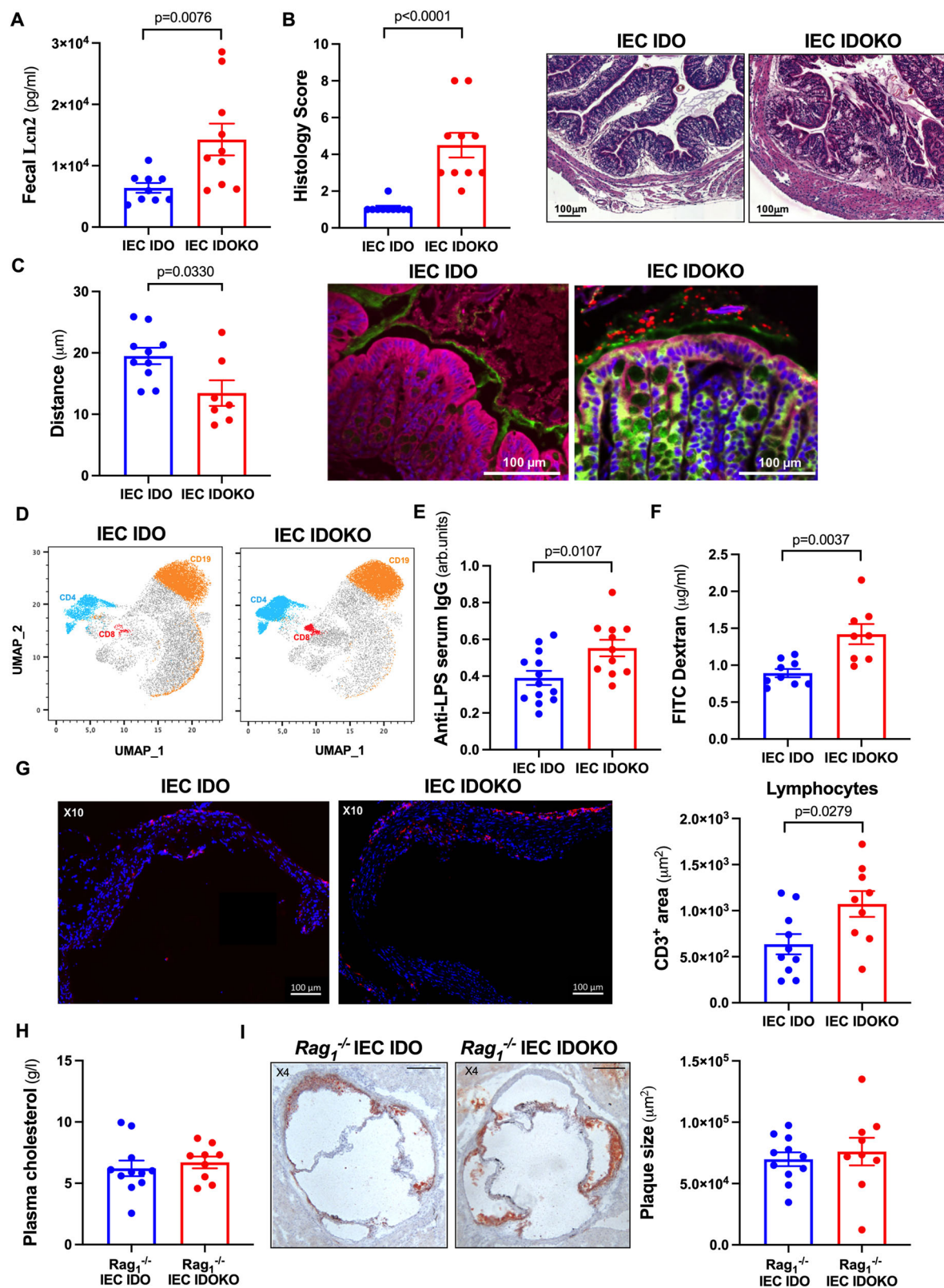
Remarkably, blockade of intestinal 5-HT production was associated with an important reduction in plaque size in the aortic sinus (Fig. 3B) and in the thoracic aorta (Supp. Fig. 8J), without any changes in plasma cholesterol levels (Supp. Fig. 8K). Moreover, atherosclerotic plaques within the aortic sinus of TPH1 inhibitor-treated mice, contained fewer inflammatory cells, including macrophages MOMA-2+ (Fig. 3C) and CD3 + T cells (Fig. 3D).

5-HT supplementation in HCD-fed male $Ldlr^{-/-}$ mice increased intestinal permeability, as assessed by augmented serum FITC-dextran 4KDa after oral gavage, and enhanced atherosclerosis, without any significant changes in plasma cholesterol levels between the 2 groups (Supp. Fig. 9A-D). Serum FITC-dextran and blood 5-HT levels were positively correlated with plaque size (Supp. Fig. 9E-F), suggesting a pro-atherogenic role of 5-HT.

Fig. 2 | Deficiency of IDO in intestinal epithelial cells (IECs) increases intestinal and plaque inflammation. A fecal lipocalin 2 (Lcn2) levels scoring in male $Ldlr^{-/-}$ IEC IDO KO ($n = 10$ mice) and littermate control $Ldlr^{-/-}$ IEC IDO ($n = 9$ mice). **B** colon pathohistological scoring in male $Ldlr^{-/-}$ IEC IDO KO and littermate control $Ldlr^{-/-}$ IEC IDO mice ($n = 10$ mice/group), after 8 weeks of high-fat and high-cholesterol diet (HFD + HCD) feeding period; scale bar 100 μm. **C** Representative confocal microscopy pictures of microbiota localization: Mucin 2 (green), actin (purple), bacteria (red), and nuclei (blue) and quantifications of mean distances of the closest bacteria (in red) to colonic IEC per condition over three high-powered fields per mouse (IEC IDO $n = 10$ mice, IEC IDOKO $n = 7$ mice); scale bar 100 μm. **D** data were acquired by flow cytometry for Uniform Manifold Approximation and Projection (UMAP) of lymphocytes in the lamina propria of the small intestines. **E** plasma anti-LPS IgG by ELISA, arbitrary units (arb. units). The results are from male $Ldlr^{-/-}$ IEC IDO KO ($n = 11$ mice) and littermate control $Ldlr^{-/-}$ IEC IDO mice ($n = 13$ mice) fed HFD + HCD for 8 weeks. **F** Detection by ELISA of FITC-dextran in serum of female $Ldlr^{-/-}$ IEC IDO KO ($n = 8$ mice) and littermate control $Ldlr^{-/-}$ IEC IDO ($n = 9$ mice) fed HFD + HCD for 13 weeks. **G** Representative photomicrographs and quantitative analysis of lesional T cells (CD3+ in red) accumulation in the aortic sinus of male $Ldlr^{-/-}$ IEC IDO KO ($n = 9$ mice) and littermate control $Ldlr^{-/-}$ IEC IDO ($n = 10$ mice), after 8 weeks of HFD + HCD feeding period; scale bar 100 μm. **H** plasma cholesterol, **I.** representative pictures, and quantifications of plaque size in the aortic sinus in male $Ldlr^{-/-}Rag_1^{-/-}$ IEC IDO KO ($n = 9$ mice) and littermate control $Ldlr^{-/-}Rag_1^{-/-}$ IEC IDO ($n = 11$ mice) fed HFD + HCD for 8 weeks; scale bar 200 μm. Individual data are presented as scattered dot plots, with the mean and s.e.m. The p values were determined using the two-tailed Mann-Whitney test. Source data are provided as a Source Data file.

Taken together, these results indicate that intestinal 5-HT exerts pro-inflammatory and pro-atherogenic effects.

Considering the observed pro-atherogenic role of intestinal 5-HT, we hypothesized that the possible increase in 5-HT in the absence of intestinal IDO may explain the pro-atherogenic phenotype of IEC IDOKO mice. We therefore examined intestinal 5-HT levels in male $Ldlr^{-/-}$ IEC IDOKO mice and littermate controls after 8 weeks of HFD + HCD. As expected, considering the availability of Trp for the other catabolic pathways, the absence of IDO in IECs led to a significant increase in 5-HT production (Supp. Fig. 10A). Interestingly, we found a correlation between 5-HT levels within the small intestine and plaque size in these mice (Supp. Fig. 10B). Then we sought to investigate whether increased plaque size in the absence of intestinal IDO was due to the observed increase in 5-HT production. To this end, we inhibited TPH1 in both male $Ldlr^{-/-}$ IEC IDOKO and $Ldlr^{-/-}$ IEC IDO mice fed HFD + HCD for 8 weeks. In agreement with the above results, TPH1 inhibition in both $Ldlr^{-/-}$ IEC IDO and $Ldlr^{-/-}$ IEC IDO KO mice led to a significant decrease in plaque size in the aortic sinus (Fig. 3E), without any significant changes in plasma cholesterol levels (Supp. Fig. 10C). Moreover, TPH1 inhibition led to a marked decrease in intestinal inflammation in IEC IDOKO mice, as assessed by a low colon histological scoring (Fig. 3F) and fecal Lcn2 levels (Fig. 3G). In agreement with the 5-HT pro-atherogenic role, we observed a significant correlation between blood 5-HT levels and plaque size in the aortic sinus (Supp. Fig. 10D). Although TPH1 inhibition significantly reduced plaque size in $Ldlr^{-/-}$ IEC IDO KO mice, there was still a trend towards larger plaque size in $Ldlr^{-/-}$ IEC IDO KO mice treated with TPH1 inhibitor compared to littermate controls treated with TPH1 inhibitor (Fig. 3E), suggesting the involvement of also other mechanisms in the pro-atherogenic phenotype associated with IDO deficiency in IECs.

Trp-dependent microbiota modulation impacts atherosclerosis

Accumulating evidence showed that intestinal cells along with immune cells interact with gut microbiota to determine disease outcomes[27]. We therefore hypothesized that intestinal IDO activity might shape gut microbiota, and promote systemic inflammation and atherosclerosis. We first explored the bacterial fecal composition of the microbiota by the use of 16 S rDNA sequencing of male $Ldlr^{-/-}$ IEC IDOKO and $Ldlr^{-/-}$ IEC IDO mice fed either HFD + HCD or NCD for 8 weeks. Principal coordinates analysis (PCoA) based on microbiota composition revealed significant differences between the groups of mice (Supp. Fig. 11A). In agreement with the deleterious effects of HFD on microbiota[28], the alpha-diversity analysis showed decreased diversity and richness under HFD + HCD compared to NCD, but no significant differences were observed according to the mice genotypes (Supp. Fig. 11B). At family levels, there were differences in relative abundance between groups (Supp. Fig. 11C). Fecal SCFA measurements in these groups showed only a decrease in fecal acetate levels in $Ldlr^{-/-}$ IEC IDOKO mice compared to littermate controls fed NCD (Supp. Fig. 11D). Under HFD + HCD condition, the levels of acetate decreased, but no significant difference was observed between the genotypes (Supp. Fig. 11D).

To address the importance of the microbiota, we depleted gut microbiota in $Ldlr^{-/-}$ IEC IDOKO and $Ldlr^{-/-}$ IEC IDO male mice fed HFD + HCD using a broad-spectrum antibiotic cocktail (ATB) supplemented in the drinking water. In agreement with previous studies[29], depletion of microbiota with ATB aggravated atherosclerosis due to enhanced plasma cholesterol levels. Moreover, ATB treatment abrogated the differences in plaque size without significant differences in plasma cholesterol, as well as gut inflammation as assessed by Lcn-2 levels, in male $Ldlr^{-/-}$ IEC IDO and $Ldlr^{-/-}$ IEC IDOKO mice fed HFD + HCD (Fig. 4A, B and Supp. Fig. 12A). Then, we wanted to test whether microbiota exchange between the two mouse genotypes might impact atherosclerosis. To this end, HFD + HCD-fed $Ldlr^{-/-}$ IEC IDO and $Ldlr^{-/-}$ IEC IDO KO mice were co-housed after weaning and compared to mice housed in cages separated according to the genotype. As shown in Fig. 4C, atherosclerosis plaque size in the aortic sinus of co-housed animals (whether $Ldlr^{-/-}$ IEC IDO or $Ldlr^{-/-}$ IEC IDO KO) was similar to those of $Ldlr^{-/-}$ IEC IDO KO mice housed in separate cages without significant changes in plasma cholesterol levels between the groups (Supp. Fig. 12B), suggesting a dominant pro-atherogenic effect of microbiota from $Ldlr^{-/-}$ IEC IDO KO mice. Then, as Trp is catabolized through microbiota-generated indole metabolites, we assessed whether the absence of IDO in IECs might alter indole production. However, unexpectedly considering the availability of Trp for the indole pathway in IEC IDOKO, lack of IDO in IECs led to a decrease in indole production, as assessed by low levels of fecal IAA (Supp. Fig. 12C). Trp is metabolized by gut bacteria into indole derivatives that activate aryl hydrocarbon receptor (AhR)[7]. We then measured AhR agonists (such as IAA, IAld, and tryptamine) in feces of $Ldlr^{-/-}$ IEC IDO and $Ldlr^{-/-}$ IEC IDO KO mice separated by genotype, and in feces of mice co-housed after weaning, as well as in mice separated by genotype but treated with ATB. As shown in Supp. Fig. 12D, a decrease in AhR agonists (IAA, IAld, and tryptamine) was observed in $Ldlr^{-/-}$ IEC IDO KO compared to $Ldlr^{/}$ IEC IDO mice, whereas this difference was abrogated in the cohoused mice. As expected given the specific production of indole derivatives by bacteria, AhR agonists (IAA, IAld, and tryptamine) markedly decreased in $Ldlr^{-/-}$ IEC IDO KO and $Ldlr^{-/-}$ IEC IDO mice treated with ATB (Supp. Fig. 12D). Noteworthy, among indole-producing bacteria[30], *Parabacteroides distasonis* relative abundance decreased in IEC IDO KO mice, and showed a positive correlation with fecal IAA levels and an inverse correlation with plaque size in control and $Ldlr^{-/-}$ IEC IDOKO mice fed HFD + HCD (Supp. Fig. 12E-G).

To investigate the physiological importance of impaired microbiota AhR activity, 6-formylindolo(3,2-b)carbazole (Ficz), an AhR agonist, was administered to HCD-fed female $Ldlr^{-/-}$ mice. Ficz treatment decreased colonic histological scoring (Fig. 4D) and alleviated atherosclerosis in the aortic sinus without any significant changes in plasma cholesterol levels (Fig. 4E, F), compared to untreated counterparts. This was associated with a decrease in CD3+ T cell accumulation within plaques (Fig. 4G), without significant changes in macrophage MOMA-
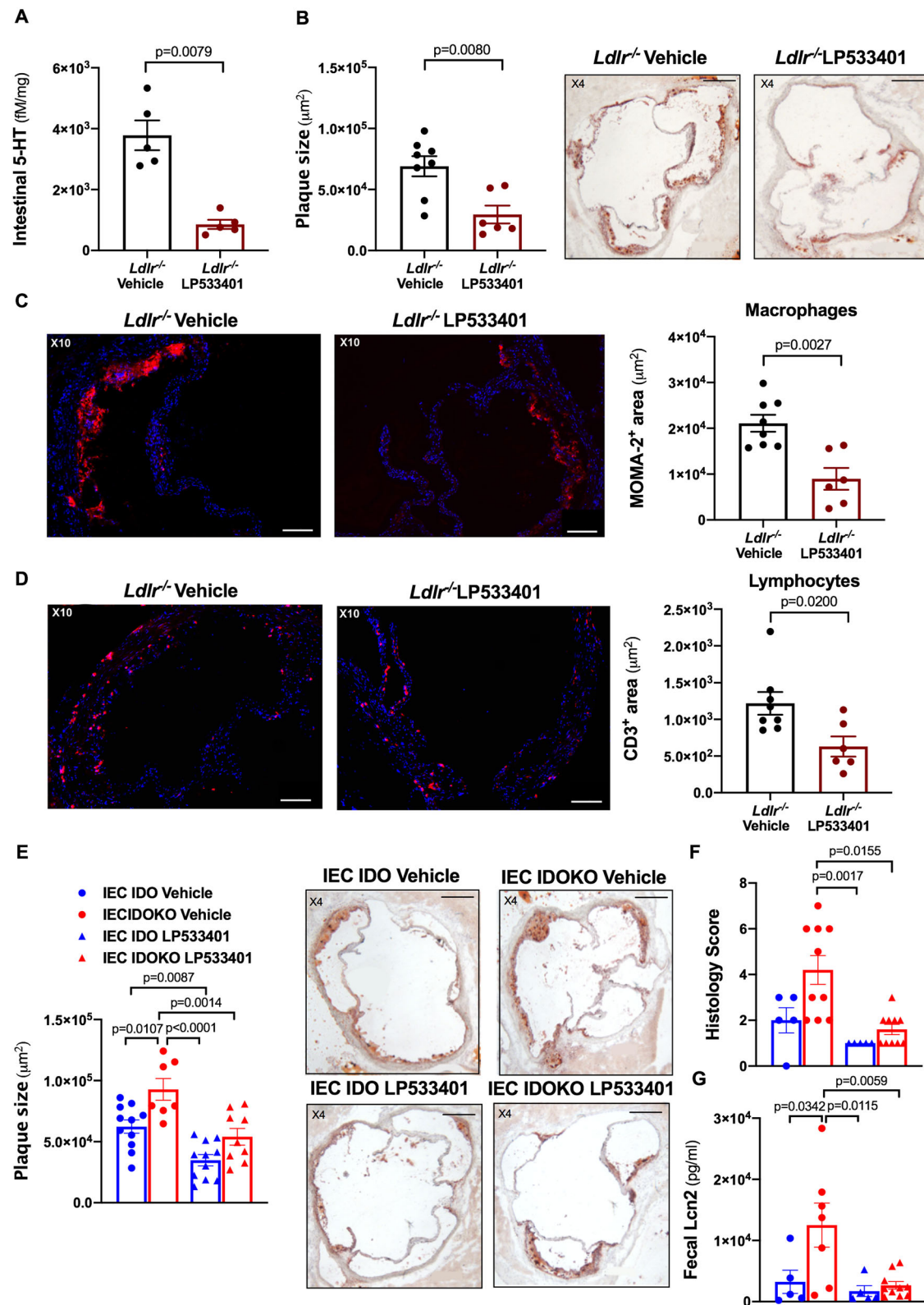
2[+] surface area (Supp. Fig. 13A). Moreover, to test the effects of indoles in atherosclerosis, we supplemented bacterial AhR agonists (a mixture of IAA, IPA, and tryptamine) to HCD-fed female $Ldlr^{-/-}$ mice for 8 weeks. Indole supplementation led to the significant increase in the fecal levels of these indole derivatives without any significant changes in intestinal 5-HT or intestinal IDO activity (Kyn/Trp) (Fig. 5A and Supp. Fig. 13B). Indole supplementation was also associated with decreased leukocyte (CD45 +) numbers in the intestine, particularly

macrophages (CD64 +), T (CD4 + , CD8 +) cells, and B (CD19 +) cells (Fig. 5B and Supp. Fig. 13C). This was accompanied by a significant decrease in plaque size in the aortic sinus without significant changes in plasma cholesterol levels (Fig. 5C, D). The decrease in atherosclerosis in the indole-supplemented group was also observed in the thoracic aorta (Fig. 5E). This was associated with a decrease in lesional macrophages MOMA2+ (Fig. 5F). Assessment of Th polarization, including Th1 (T-bet +), Th17 (ROR-γt +), and Treg (Foxp3 +) subsets

Fig. 3 | Intestinal 5-hydroxytryptamine (5-HT) exhibits pro-inflammatory and pro-atherogenic effects. A 5-HT levels in small intestine extracts ($n = 5$ mice/group), **B** plaque quantification in the aortic sinus and representative images of male $Ldlr^{-/-}$ treated with Tryptophan Hydroxylase 1 (TPH1) inhibitor (LP533401, $n = 6$ mice) or vehicle ($n = 8$ mice) and fed HFD + HCD for 8 weeks; scale bar 200 μm. **C, D** representative images and quantifications of macrophages (MOMA-2+ in red) and lymphocytes (CD3+ in red) accumulation in the aortic sinus ($Ldlr^{-/-}$ Vehicle $n = 8$, $Ldlr^{-/-}$ LP533401 $n = 6$); scale bar 100 μm. **E** representative pictures and quantifications of plaque size in the aortic sinus male $Ldlr^{-/-}$ IEC IDO KO and littermate control $Ldlr^{-/-}$ IEC IDO mice treated with either LP533401 or vehicle and fed HFD + HCD for 8 weeks (IEC IDO Vehicle $n = 11$ mice, IEC IDO KO Vehicle $n = 7$ mice,

IEC IDO LP533401 $n = 11$ mice, IEC IDO KO LP533401 $n = 9$ mice); scale bar 200 μm. **F** Colon pathohistological scoring (IEC IDO Vehicle $n = 5$ mice, IEC IDO KO Vehicle $n = 10$ mice, IEC IDO LP533401 $n = 5$ mice, IEC IDO KO LP533401 $n = 10$ mice). **G** lipocalin-2 (Lcn2) levels in feces (IEC IDO Vehicle $n = 5$ mice, IEC IDO KO Vehicle $n = 7$ mice, IEC IDO LP533401 $n = 5$ mice, IEC IDO KO LP533401 $n = 10$ mice). Individual data are presented as scattered dot plots, with the mean and s.e.m. The p values were determined using the two-tailed Mann-Whitney test for **A**–**D**, Kruskal-Wallis, followed by post-Hoc Dunn's test for **F**, and one-way ANOVA test followed by Tukey's multiple comparison test for **E** and **G**. Source data are provided as a Source Data file.

in the small intestines, Peyer's Patches (PP), mesenteric lymph nodes (MLNs), and spleens, showed only a significant increase in Th17 in PPs from indole-treated mice compared to controls (Supp. Fig. 14 and 15).

Taken together, these results point to the importance of microbiota, particularly bacteria-produced indoles, and AhR-mediated effects in atherosclerosis.

Discussion

Trp is one of the nine essential amino acids from dietary origin and whose metabolism has major effects on host functions[9]. IDO is the main pathway for degrading Trp in the extrahepatic compartments[31]. Although IDO has previously been reported to be highly expressed in the gastrointestinal tract[32], together with the ascertainment of the importance Trp metabolism for intestinal homeostasis[4], the specific role of intestinal IDO has not yet been explored. During inflammation, IDO is classically known to be up-regulated in myeloid cells by pro-inflammatory stimuli, such as LPS and interferon (IFN)-γ[33]. IDO is an upstream enzyme that is involved in the generation of Kyn and thereafter, following a cascade of different enzymatic reactions, Kyn-derived metabolites that exert either protective or deleterious effects[34]. As a protective role, IDO through Kyn metabolite, has been described as an immunosuppressive enzyme that inhibits effector T-cell function and favors the differentiation of Tregs[35]. This seems to be highly relevant during infection and pregnancy settings[36]. However, in our study, the absence of IDO in IEC did not significantly impact intestinal Treg polarization, which may indicate that this would not be the primary mechanism. Accordingly, Kyn supplementation in intestinal IDO-deficient mice did not significantly impact atherosclerotic plaque size.

The biological effects of IDO are not limited to the regulation of the immune response. IDO activity has been shown to contribute to arterial vessel relaxation and to the control of blood pressure in septic shock[37]. IDO activity was also shown to play a critical role in aneurysm[38,39] as well as in obesity[13] and acute myocardial infarction[40].

In the last decades, a number of experimental studies have been conducted to elucidate the role of IDO in inflammatory intestinal diseases, but contradictory results have been reported[41]. The discrepancies regarding the role of IDO in IBD might be explained by differences in mouse models and experimental settings used to induce colitis. In atherosclerosis, the findings of previous studies using global deletion of IDO have been controversial, showing both proatherogenic[10,11] or atheroprotective effects[12]. Our prior work has shown that under HCD condition IDO expressed in myeloid cells exerted a pro-atherogenic role through kynurenic acid[12]. Yet, it is noteworthy that under HCD condition IDO is weakly induced in the gut, as shown in the present study, which suggests that the observed phenotype of mice fed HCD with global deficiency of IDO was independent of IDO expression in the gut.

IDO seems to play a versatile role that might be due to the tissue-specific effects of this enzyme, suggesting that its function is tailored to the tissue/organ and the microenvironment in different pathological settings. Understanding the role of intestinal IDO is particularly

important since the Trp metabolism in the gut is specific insofar as serotonin and microbiota-produced indoles are mainly produced in the gut[9]. Herein, we showed that the specific deletion of IDO in IECs led to a marked decrease in its activity in the small intestine, indicating that the expression of IDO in IECs is crucial for its activity in the gastrointestinal tract. Intestinal IDO deficiency resulted in augmented intestinal and peripheral inflammation that likely accounted for increased atherosclerosis. This was associated with a high number of lymphocyte accumulation within the atheromatous plaques. Moreover, the proatherogenic role due to intestinal IDO deficiency was highly dependent on lymphocytes as the phenotype was abrogated in lymphocyte-deficient mice.
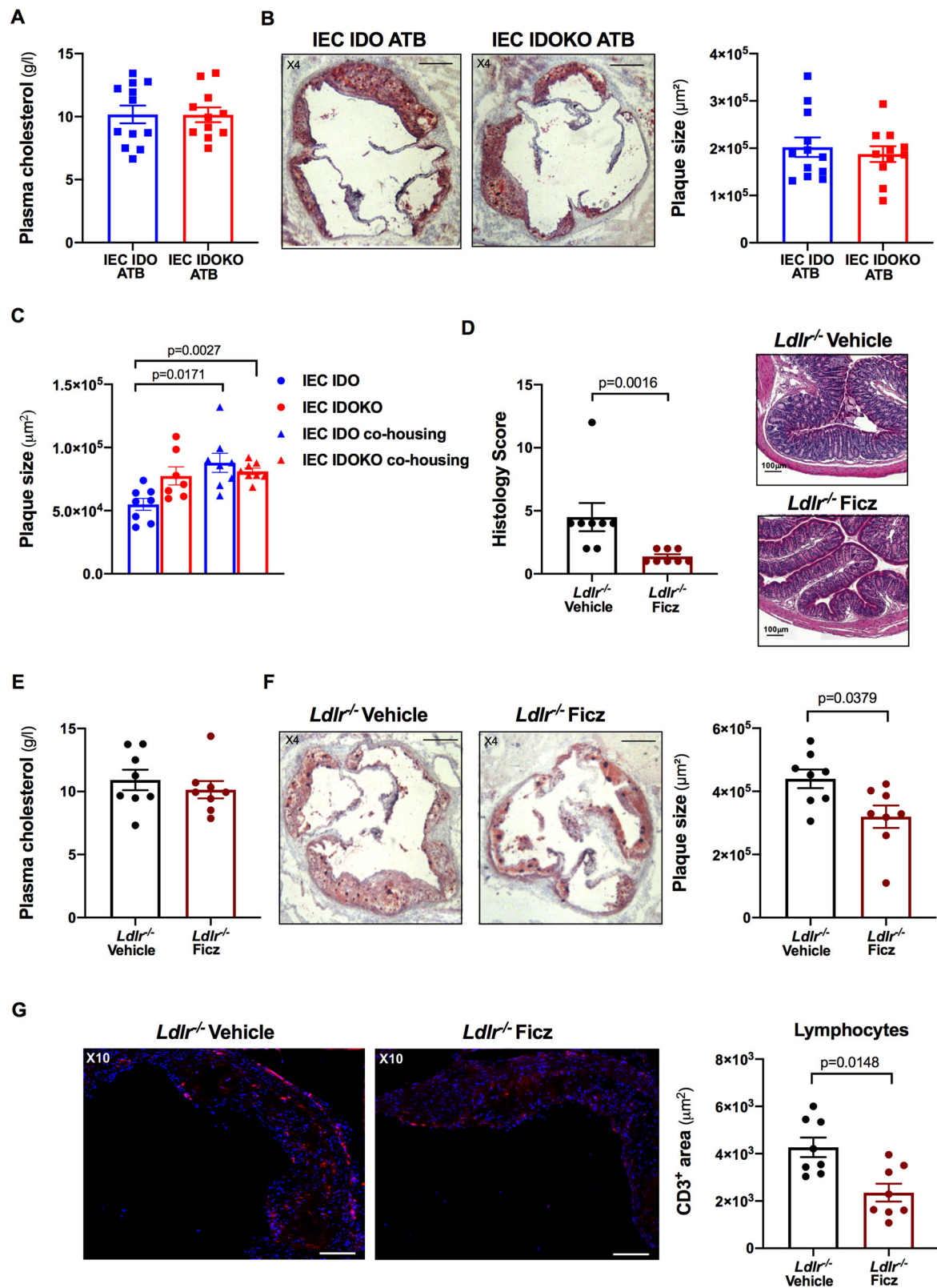
The Kyn, indole, and 5-HT pathways are interrelated in such a way that they depend on the use of Trp[9]. This makes it difficult to dissect the functional impact of each pathway, as the change of one catabolic pathway impacts the others. Therefore, as expected, the absence of IDO in intestinal cells led to an increase in 5-HT production. However, unexpectedly, IEC IDOKO mice showed decreased indole production, while increased production was expected since more Trp was available for this pathway as a result of Kyn pathway blockade. The most likely explanation for this observation is that the lack of IDO in intestinal cells decreased indole-produced bacteria and/or promoted the expression of IDO in gut leukocytes, which ultimately hijacked Trp. In agreement with this hypothesis, we observed an increase in IDO expression in leukocytes isolated from the intestines of IEC IDO KO mice. We also observed a decrease in the relative abundance of one bacteria involved in indole production[30] *Parabacteroides distasonis*, which abundance positively correlated with fecal IAA levels and negatively with plaque size.

Although these observations could account for decreased indole production in IEC IDOKO mice, the precise mechanisms responsible for the changes in microbiota and thus indole production remain to be further investigated. Moreover, whether the observed decrease in indole levels in IEC IDO KO was directly involved in the observed increase in atherosclerosis remains to be further examined.

IDO expression within the small intestines during atherosclerosis was different according to gender, suggesting sex hormone regulation of IDO expression within the gut. In particular, there was an inverse significant correlation between the gene expression of IDO and estrogen receptor 2 in the small intestines, suggesting a negative regulation of IDO expression in the gut through this receptor, which is in agreement with a previous study in cancer cells[42]. However, as there are no estrogen response elements on the *Ido1* promoter sequence, we believe that the effect of estrogens on *Ido1* expression in the gut is indirect, which required further studies to decipher the mechanisms behind how estrogens could modulate intestinal IDO-mediated effects on atherosclerosis.

The IEC IDO-dependent anti-atherogenic effect was revealed in conditions of HFD combined with HCD, but not in conditions of HCD alone, which can be accounted for by the fact that intestinal IDO activity was markedly induced by HFD, but not by HCD. HFD-mediated upregulation of intestinal IDO most likely resulted from an HFD-driven decrease in the production of SCFA, especially butyrate that has been

A Plasma cholesterol (g/l) — IEC IDO ATB vs IEC IDOKO ATB

B IEC IDO ATB / IEC IDOKO ATB (X4); Plaque size (µm²) — IEC IDO ATB vs IEC IDOKO ATB

C Plaque size (µm²); p=0.0027; p=0.0171; IEC IDO, IEC IDOKO, IEC IDO co-housing, IEC IDOKO co-housing

D Histology Score — $Ldlr^{-/-}$ Vehicle vs $Ldlr^{-/-}$ Ficz; p=0.0016; $Ldlr^{-/-}$ Vehicle / $Ldlr^{-/-}$ Ficz (100 µm)

E Plasma cholesterol (g/l) — $Ldlr^{-/-}$ Vehicle vs $Ldlr^{-/-}$ Ficz

F $Ldlr^{-/-}$ Vehicle / $Ldlr^{-/-}$ Ficz (X4); Plaque size (µm²); p=0.0379

G $Ldlr^{-/-}$ Vehicle / $Ldlr^{-/-}$ Ficz (X10); Lymphocytes; CD3$^+$ area (µm²); p=0.0148

reported to down-regulate *Ido1* expression in IECs[16]. Consistently, supplementation of HFD with soluble fibers, which increased butyrate levels, down-regulated IDO activity, as shown by decreased Kyn levels in this condition.

The HFD-mediated increase in intestinal IDO activity might participate in a negative feedback loop to limit inflammatory responses caused by HFD.

HFD has many other pathogenic effects. Particularly, we found that HFD alleviated indole production, in agreement with previous studies[13,14]. Microbiota-derived indole metabolites promote intestinal barrier integrity and immune cell homeostasis, which has been shown to play a protective role in obesity[13,14], and IBD[43]. The protective roles of indole metabolites in maintaining intestinal barrier integrity and immune cell homeostasis seem, at least in part, to be dependent on the

Fig. 4 | Trp-dependent microbiota effects impact atherosclerosis. A Plasma cholesterol, **B** representative pictures and quantifications of plaques in the aortic sinus of male *Ldlr*^{-/-} IEC IDO KO and littermate control *Ldlr*^{-/-} IEC IDO mice treated with antibiotics (ATB) during the 8 weeks of high-fat and high-cholesterol diet (HFD + HCD) feeding period (IEC IDO ATB *n* = 12 mice, IEC IDO KO ATB *n* = 11 mice); scale bar 200 µm. **C** plaque quantification in the aortic sinus of male *Ldlr*^{-/-} IEC IDO KO and littermate control *Ldlr*^{-/-} IEC IDO mice either separated by the genotype or mixed (co-housing) in the same cages from the weaning. The mice were fed HFD + HCD for 8 weeks (IEC IDO *n* = 8 mice, IEC IDO KO *n* = 7 mice, IEC IDO co-housing *n* = 8 mice, and IEC IDO KO co-housing *n* = 8 mice). **D** colon pathohistological scoring; scale bar 100 µm, **E** plasma cholesterol levels, **F** representative pictures and quantifications of plaque size in the aortic sinus; scale bar 200 µm, **G** representative pictures and quantifications of lymphocytes (CD3+ in red) accumulation within plaques in the aortic sinus of male *Ldlr*^{-/-}mice treated with 6-Formylindolo(3,2-b)carbazole (Ficz) or vehicle; scale bar 100 µm (*n* = 8 mice/group) during the 8 weeks of HCD feeding period. Individual data are presented as scattered dot plots, with the mean and s.e.m. The *p* values were determined using the two-tailed Mann-Whitney test. Source data are provided as a Source Data file.

activation of AhR and the production of interleukin (IL)-22[3,7]. The transcription factor, AhR a well-known receptor for indole metabolites (such as IAA, IPA, and tryptamine), has been reported to promote intestinal homeostasis and suppress inflammation[44]. Recently, one of the indole metabolites, IPA, has been shown to protect against atherosclerosis[45]. In agreement with these observations, we found that the supplementation with Ficz, an AhR agonist, as well as indole metabolites, relieved intestinal inflammation and decreased atherosclerosis.

5-HT is another important Trp-derived metabolite that plays key roles in gut function. Although serotonin is considered as an important central physiologic mediator of intestinal function by regulating gut motility, permeability, and other functions, accumulating evidence point to its potent inflammatory effects[46]. The increase in 5-HT acts as a pro-inflammatory factor within the gut, as evidenced by studies showing that blocking 5-HT production with LP533401, a small molecule inhibitor of TPH1, an enzyme responsible for the synthesis of gut-derived serotonin, reduced inflammation in colitis models, without affecting the brain serotonin content[46]. The inflammatory role of 5-HT in the gut seems likely related to nuclear factor-kappa B (NF-κB) induction[25].

5-HT levels were also associated with CVD and thought to exert a deleterious role[46], although its role in atherosclerosis has been poorly investigated.

We found that daily injection of LP533401 resulted in a marked decrease in 5-HT levels in both the gut and blood, compared to vehicle-treated mice. TPH1 inhibition reduced atherosclerosis and alleviated intestinal and plaque inflammation. The protective role of TPH1 inhibition was also observed in IEC IDOKO mice as evidenced by our results showing the decrease in gut and plaque inflammation as well as atherosclerosis in this mouse model. Moreover, 5-HT supplementation led to an increase in intestinal permeability and atherosclerosis, confirming the pro-atherogenic role of 5-HT.

In conclusion, our data uncover the pivotal role of intestinal Trp-dependent pathways in gut inflammation and, as a result, in atherosclerosis development, thereby contributing to a better understanding of the link between the gut and the periphery, and unveiling this metabolic pathway as a potential therapeutic target.

Methods

Mice

All experiments were conducted according to the ethical committee for animal experimentation (University of Paris Cité, CEEA 34) and the National Charter on the ethics of animal experimentation from the French Minister of Higher Education and Research under the reference MESR no. 01373.01. All mice were bred in specific pathogen-free laboratory animal facilities under standard conditions with temperatures of 21–23 °C, 40–60% humidity, and 12 h light/dark cycles. Animals were provided with food and water ad libitum. Both male and female mice at the age of 8 weeks were used in this study. We implemented reduction and refinement principles to minimize harm to the animals. Procedures were used to minimize pain, suffering, and distress for the mice, ensuring their welfare is prioritized. This includes improving housing conditions, using less invasive techniques, and providing effective analgesia and anesthesia. Before euthanasia by cervical dislocation, animals were anesthetized with isoflurane (3% in oxygen).

Ldlr^{-/-} (JAX:002207), *Rag₁*[-/-] (JAX:002216), *Villin-cre*^{+/-} (JAX:004 586) mice were bought from the Jackson Laboratory and bred in our facility. *Rag₁*[-/-] mice were crossed with *ldlr*^{-/-} mice to obtain *Rag₁*[-/-] *ldlr*^{-/-} mice. *Ido-1*[flox/flox] mice were kindly given by Marc Veldhoen (Babraham Institute Cambridge). *Ido-1*[flox/flox] mice were crossed with *Villin-cre*[+/-]mice. Then the resulting mice were crossed with *Ldlr*^{-/-} to obtain *ldlr*^{-/-} *Ido-1*[flox/flox]*villin-cre* mice. *ldlr*^{-/-} *Ido-1*[flox/flox]*villin-cre* + /– and littermate *ldlr*^{-/-} *Ido-1*[flox/flox]*villin-cre*–/– control mice were used in some experiments. *Rag₁*[-/-] *ldlr*^{-/-} mice were crossed with *ldlr/ Ido-1*[flox/flox]*villin-cre* mice to obtain *Rag₁*[-/-] *ldlr*^{-/-} *Ido-1*[flox/flox]*villin-cre* mice. *Rag₁*[-/-] *ldlr*^{-/-} *Ido-1*[flox/flox]*villin-cre* + /– mice and littermate *Rag₁*[-/-] *ldlr*^{-/-} *Ido-1*[flox/flox]*villin-cre*–/– control mice were used in some experiments. All mice were on C57Bl/6 background and were backcrossed for more than 10 generations. In general, mice (*n* = 5/cage) were separated by genotype at weaning until the sacrifice. In co-housing experiments, 4 mice (*n* = 2 per genotype) were mixed in the same cages from the weaning until the sacrifice.

Mice were fed with either a normal chow diet (NCD) (A03, SAFE, France) or subjected to high-fat diet (HFD) containing 60% FAT (E15742-347, SSNIFF, Germany) or a high-cholesterol diet (HCD) containing 1.25% cholesterol (E15106-347, SSNIFF, Germany) or a combination of both HFD + HCD diet (SSNIFF, Germany) (composition shown in Supp. Figure 1A). A specific diet was started at 7 weeks of age and continued for 13 weeks or less with ad libitum access to water and food. In some experiments, FOS (Fructooligosaccharides), as a source of soluble dietary fibers was diluted in drinking water (7.5%). Gut microbiota was depleted using a combination of oral antibiotics (metronidazole 1 g/L, amoxicillin 0.5 g/L, vancomycin 0.5 g/L, neomycin 1 g/L) dissolved in drinking water with sucralose (4 g/L)[47]. In other experiments, kynurenine or indole derivatives (IAA, IPA, and tryptamine) or the 5-HT precursor, L-5-hydroxytryptophane (5-HTP) (2 mg/ml diluted in drinking water, Sigma-Aldrich) supplementation to *ldlr*^{-/-} or *ldlr*^{-/-} *Ido-1*[flox/flox]*villin-cre* mice was performed for 8 weeks of HFD + HCD or HCD. A group of mice was injected with the 6-formylindolo(3,2-b)carbazole (Ficz; 1 µg/mouse, one time per week, Santa Cruz Biotechnology, USA) or vehicle along the 8 weeks of HCD. Other groups of mice were daily injected with TPH1 inhibitor LP533401 (25 mg/kg, Dalton Pharma Services, Canada) or an equal volume of vehicle along the 8 weeks of HFD + HCD feeding period. All mice used in these experiments were bred and housed in a specific pathogen-free barrier facility (the health certificate is provided in the Supp. Table 1). Animal experiments were performed according to the European directive (2010/63/UE) and to the institutional guidelines approved by the local ethics committee of the French authorities, the 'Comité d'Ethique en Experimentation Animale' (CEEA) under the following number APAFIS #33148-2021080517361889.

In vivo studies

For oral glucose tolerance test (OGTT), mice were fasted overnight prior to an oral administration of 1 g/kg glucose. Blood was sampled from the tail vein at 0, 5, 15, 30, 60, 90 and 120 min in order to assay
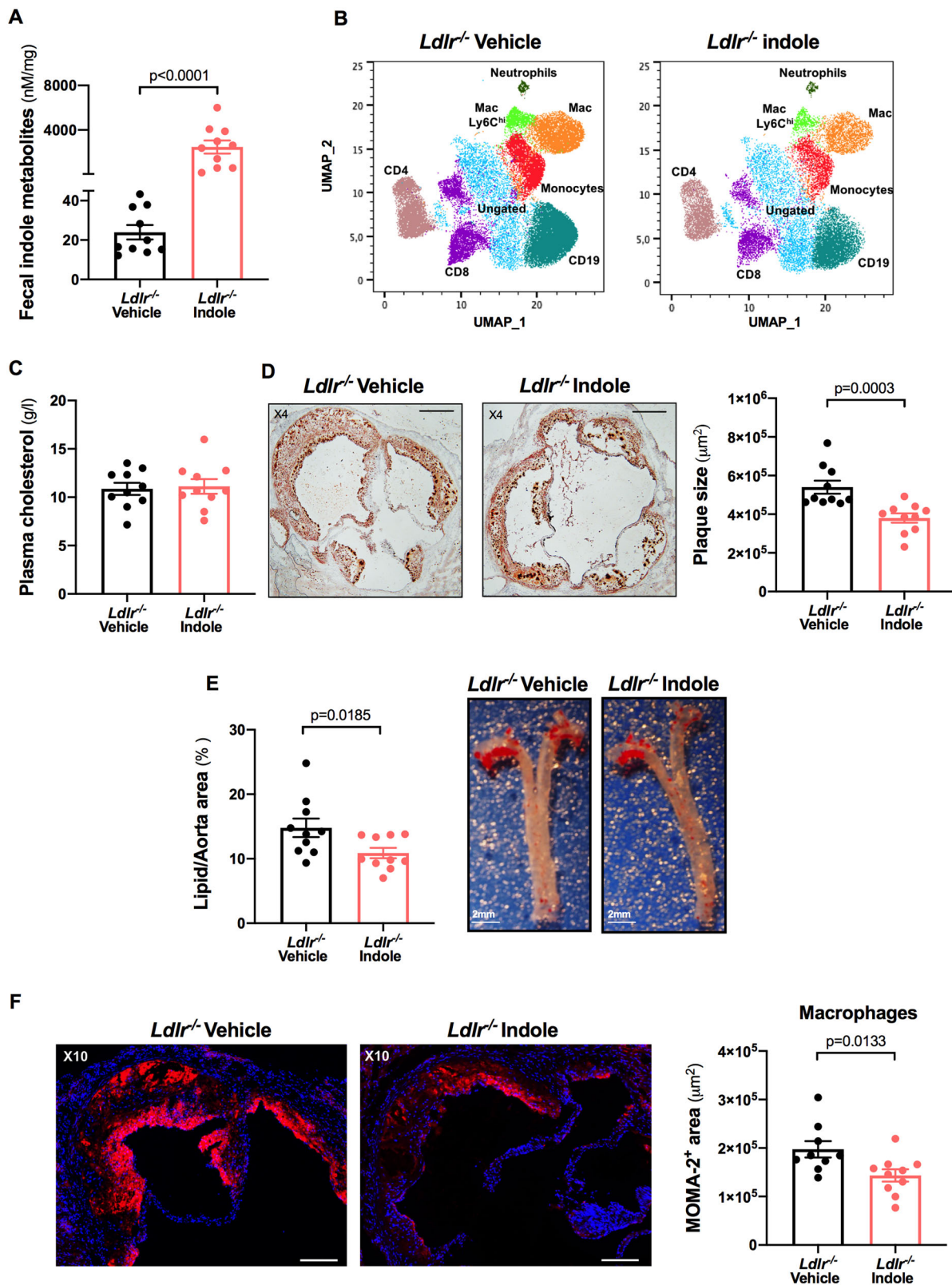
Fig. 5 | Indole derivatives alleviate inflammation and atherosclerosis. A indole derivatives (sum of IAA, IPA, and tryptamine) levels supplemented or not in female *Ldlr*^-/- mice fed a high-cholesterol diet (HCD) for 8 weeks (*n* = 10 mice/group). **B** data were acquired by flow cytometry for Uniform Manifold Approximation and Projection (UMAP) of leukocytes in the lamina propria of small intestines. Unbiased multi-dimensional analysis by X-shift revealed several different clusters. **C** plasma cholesterol levels, **D** representative pictures and plaque size quantification in the aortic sinus; scale bar 200 μm, **E** representative images and lipid quantification with en-face staining in the thoracic aorta (*n* = 10 mice/group); scale bar 2 mm, **F** representative photomicrographs and quantitative analysis of lesional macrophages (MOMA2+ in red) accumulation in the aortic sinus of female *Ldlr*^-/- mice fed HCD for 8 weeks (*Ldlr*^-/- Vehicle *n* = 9 mice, *Ldlr*^-/- Indole *n* = 10 mice); scale bar 100 μm. Individual data are presented as scattered dot plots, with the mean and s.e.m. The *p* values were determined using the two-tailed Mann-Whitney test. Source data are provided as a Source Data file.

glucose concentration (OneTouch Ultra glucometer, LifeScan Europe). At 0, 15, 30, 60 min tail vein blood was collected, plasma samples were stored at −20 °C until they were analyzed for insulin concentration (Crystal Chem Inc., Downers Grove, USA). Insulin tolerance test (ITT) was performed in mice food deprived for 5 h prior to an intraperitonal injection of 1 U/kg insulin. Blood was sampled from the tail vein at 0, 5, 15, 30, 60 and 90 min in order to assay glucose concentration.

In vivo intestinal permeability
Permeability in vivo was assessed using fluorescein isothiocyanate-conjugated dextran (FITC–dextran 3000–5000 Da, Sigma–Aldrich) tracer[7]. Briefly, at the endpoint 0.6 mg/g body weight of FITC–dextran dissolved in PBS was administered to mice by oral gavage. To measure the presence of FITC–dextran in blood, 3.5 h after the gavage blood samples were recovered from the retro-orbital venous plexus and kept in the dark at 4 °C until analysis. Serum has separated by centrifugation (5000 g, 30 minutes, 4 °C), and plasma FITC levels were determined using a fluorescence microplate reader (excitation 485 nm and emission 530 nm).

Biochemical measurements
Blood glucose level was measured using a glucometer (OneTouch Ultra, LifeScan Europe). Plasma insulin (Crystal Chem Inc., Downers Grove, USA) was determined by enzyme-linked immunosorbent assay (ELISA) (R&D Systems). HOMA-IR in mice was calculated using the equation ((fasting glucose concentration x fasting insulin concentration)/405)[48].

Fecal lipocalin-2 measurements
Frozen fecal samples were reconstituted in phosphate-buffered saline (PBS) containing 0.1% Tween 20 (100 mg/mL) and vortexed for 20 minutes to get a homogenous fecal suspension, which was then centrifuged at 18000 g and 4 °C for 10 minutes. Lipocalin-2 concentrations were measured in the supernatants using Duoset murine lipocalin-2 ELISA kit (R&D Systems, Minneapolis, MN)[21].

Serum LPS-specific immunoglobulins
Lipopolysaccharide (LPS)-specific IgG levels were quantified by ELISA. Microtiter plates were coated overnight with purified *E. coli* LPS (1 μg/well from *E. coli* 0128: B12, Sigma, Catalog No. 2887). Serum samples diluted 1:200 were then applied. After incubation and washing, wells were incubated with anti-mouse IgG-HRP. Quantification was performed using the colorimetric peroxidase substrate tetramethylbenzidine and optical density (OD) was read at 650 nm with an ELISA plate reader. Data are reported as OD corrected by subtracting background (determined by readings in samples lacking serum).

Histology
The entire mouse colon was excised, and segments of the proximal colon (1 cm) were fixed in buffered 4% formalin, paraffin embedded, cut into 4-μm sections, and stained with hematoxylin/eosin/safranin (HES). The histological severity of colitis was graded in a "blinded" fashion. The tissue samples were evaluated for the amount and depth of inflammation with a range of 0 to 3 and the amount of crypt damage or regeneration with a range of 0 to 3, as previously established[49].

Localization of bacteria by FISH
Fluorescent in situ hybridization (FISH) was performed[50], in order to analyze bacteria localization at the surface of the intestinal mucosa. Briefly, colonic tissues (proximal colon, 2nd cm from the cecum) containing fecal material were placed in methanol-Carnoy's fixative solution (60% methanol, 30% chloroform, 10% glacial acetic acid) for a minimum of 3 h at room temperature. Tissue were then washed in methanol 2 × 30 min, ethanol 2 × 15 min, ethanol/xylene (1:1) 15 min and xylene 2 × 15 min, followed by embedding in Paraffin with a vertical

orientation. Five μm sections were performed and dewax by preheating at 60 °C for 10 min, followed by xylene 60 °C for 10 min, xylene for 10 min, and 99.5% ethanol for 10 minutes. The hybridization step was performed at 50 °C overnight with EUB338 probe (5′-GCTGCCTCCCGTAGGAGT-3′, with a 5′ labeling using Alexa 647) diluted to a final concentration of 10 μg/mL in hybridization buffer (20 mM Tris–HCl, pH 7.4, 0.9 M NaCl, 0.1% Sodium Dodecyl Sulfate (SDS), 20% formamide). After washing 10 min in wash buffer (20 mM Tris–HCl, pH 7.4, 0.9 M NaCl) and 3 × 10 min in PBS, PAP pen (Sigma, St. Louis, MO) was used to mark around the section and block solution (5% fetal bovine serum in PBS) was added for 30 min at 4 °C. Mucin-2 primary antibody (rabbit H-300, Santa Cruz Biotechnology) was diluted 1:1500 in block solution and apply overnight at 4 °C. After washing 3 × 10 min in PBS, block solution containing anti-rabbit Alexa 488 secondary antibody diluted 1:1500, Phalloidin-Tetramethylrhodamine B isothiocyanate (Sigma, St. Louis, MO) at 1 μg/mL and Hoechst 33258 (Sigma, St. Louis, MO) at 10 μg/mL was applied to the section for 2 h. After washing 3 × 10 min in PBS slides were mounted using Prolong anti-fade mounting media (Life Technologies). Observations were performed with a Zeiss LSM 700 confocal microscope with software Zen 2011 version 7.1. This software was used to determine the distance between bacteria and epithelial cell monolayer.

Extent and plaque composition of atherosclerotic lesions
Mice were anesthetized with isoflurane before sacrifice. Plasma cholesterol were measured using a commercial cholesterol assay kit (DiaSys Diagnostic Systems GmbH). The heart and aorta, including the brachiocephalic artery, were taken off, fixed in 4% paraformaldehyde for 2 hours. Lipids were detected using Oil red O coloration[51]. Lesion extent in the thoracic aorta represents the percentage of Oil red O staining. For immunostaining, we used antibodies raised against MOMA-2 (MAB1852, Merck Milllipore®) and CD3 (A0452, Dako®) to detect macrophages and T cells respectively[52]. Masson's trichrome staining was performed to visualize necrotic cores[51]. Quantification within atherosclerotic lesions was performed in cross-sectional areas throughout the whole aortic sinus, which represents ~6-8 sections per mouse, and appropriate negative controls were used. Morphometric studies using Histolab software (Microvision), or ImageJ (NIH) software.

Quantitative real time PCR and NanoString technology
Intestines were lysed in detergent buffer RLT and then subjected to RNA extraction and reverse transcription (Qiagen) or NanoString technology. Quantitative real-time PCR was performed on an ABI PRISM 7700 (Applied Biosystems) in triplicates. Cycle threshold for Gapdh (primers: Gapdh-R, 5′-CGTCCCGTAGACAAAATGGTGAA-3′; *Gapdh*-L, 5′-GCCGTGAGTGGAGTCATACTGGAACA-3′) was used to normalize gene expression. Primers for *Reg3g*-R 5′-TTCCTGTCCTCCATGATCAAAA-3′ and *Reg3g*-L 5′-CATCCACCTCTGTTGGGTTCA-3′; *Reg3b*-R 5′-ATGCTGCTCTCCTGCCTGATG-3′ and *Reg3b*-L 5′-CTAATGCGTGCGGAGGGTATATTC-3; *Occludin*-R 5′-AAGGTTTCCGTCTGTCATAATCTC-3′ and *Occludin*-L 5′-TGGCTGCTGCTGATGAATATAATA 3′; *TNF-α*-R 5′-CGTGGGCTACAGGCTTGTCAG 3′ and *TNF-α*-L 5′-GATGGGGGGCTTCCAGAACT 3′, *esr1*-R 5′- CTCCCGCCTTCTACAGGTCTAA-3′ and *esr1*-L 5′-GACAGTCTCTCTCGGCCATTCT-3′, *esr2*-R 5′-GCCCTGTTACTAGTCCAAGC-3′ and *esr2*-L 5′-CAGGACCAGACACCGTAATG-3, *greb1*-R 5′-TCATTATCTGTGCCTGCCGGA-3′ and *greb1*-L 5′-CACTTTGCCAGTGACCAGCTC-3′. PCR conditions were 10 min at 95 °C; 35 cycles of 95 °C for 15 s, 60 °C for 20 s and 72 °C for 20 s and a final extension at 72 °C for 20 s. The NanoString Mouse Immunology Panel was used to profile gene expression of immunology-related genes. Briefly, RNA samples (50 ng) were hybridized with the NanoString probe sets. Then, Hybridized samples were processed on the nCounter Analysis System, which digitally counts the barcoded probe signals. Data was exported to nSolver Analysis Software for normalization and analysis.

Metabolite quantifications

Measurement of short-chain fatty acids (SCFA), including acetate and butyrate in feces was performed, as previously described[53]. Briefly, a stock solution of SCFA metabolites (Sigma Aldrich, France) was prepared and serially diluted to get 10 calibration solutions. A working solution of internal standards was prepared in 0.15 M NaOH to get the following final concentrations: 75 mmol/L of D3-acetate and 2.5 mmol/L of 13C-butyrate (Sigma Aldrich). Stool samples were weighed (~ 50 mg), dissolved in 200 µL of sodium hydroxide solution at 0.15 M (NaOH, Sigma Aldrich). Twenty microliters of the internal standard solution were added to stool samples and calibration solutions. Each sample was then acidified with 5 µL of hydroxide chloride 37% (Sigma Aldrich, France) and then extracted with 1.7 mL of diethyl ether (Bio-solve, France). Samples were stirred gently for 1 hour and then centrifuged 2 min (3000 g, 4 °C). The organic layers were transferred into 1.5 ml glass vials, and SCFAs were derivatized with 20 µL of tert-butyldimethylsilyl imidazole (Sigma Aldrich, France). Samples were heated at 60 °C for 30 minutes before analysis using an Agilent Technologies gas chromatography system (model 7890A-5975C, France). The temperature program started at 50 °C for 1 min, ramped to 90 °C at 5 °C/min, then up to 300 °C at 70 °C/min.

L-Tryptophan (Trp) and L-Kynurenine (Kyn), and serotonin or 5-hydroxytryptamine (5-HT) levels were measured via liquid chromatography using a coulometric electrode array (ESA Coultronics, ESA Laboratories, Chelsford, MA, USA)[54]. Quantifications were performed by referencing calibration curves obtained with internal standards.

Metabolites were extracted from the fecal pellets using a methanol/chloroform extraction method[55] with minor modifications. Cold methanol/chloroform (2:1, v/v; 1.5 ml) was added to a preweighed cecal or fecal sample and homogenized on ice. The sample tube was centrifuged at 15,000 g for 10 minutes at 4 °C, and the supernatant was transferred to a new sample tube through a 70-mm cell strainer. Ice-cold water (0.6 ml) was added, and the sample tube was vortexed and centrifuged (15,000 g, 5 minutes, 4 °C) to obtain phase separation. The upper and lower phases were separately collected in fresh sample tubes with a syringe, taking care not to disturb the interface. The polar (upper) phase (500 ml) was evaporated to dryness in a Savant Speed-Vac concentrator (Thermo Scientific, Asheville, NC), and then was reconstituted in 50 ml of methanol/water (1:1, v/v). Extracted metabolites were stored at -80 °C until analysis. Indole-3-acetic (IAA), Indole-3-propionic acid (IPA), Indole-3-aldehyde (IAld), indole, and tryptamine were quantified via liquid chromatography coupled to mass spectrometry (LC-MS) and/or via liquid chromatography coupled to a fluorescence detector (LC-Fluo) by using a Shimadzu Prominence. The LC system is equipped with a binary solvent delivery manager and sample manager (Shimadzu, Kyoto, Japan) and that was coupled to a triple quadrupole (TQ-MS) mass spectrometer equipped with an electrospray interface (ESI) for LC-MS or with a fluorescence detector (RF20Ax, Shimadzu) for LC-Fluo. The fluorescence detection was carried out simultaneously at three different excitation wavelengths: 280, 344, and 309 nm and the emission wavelength was set at 330 or 398 nm. Compounds (IAld, IAA, IPA, and tryptamine) were identified by comparing with the retention time of reference standards in our in-house library. For LC-MS the quantification was done on Multiple reaction monitoring (MRM) mode and MRM transitions for IAA, IPA, and indole are used as follows: 173 > 129; 190 > 130; 118 > 91. The quantification was done by integration of the peak absorbance area, employing a calibration curve established with various known concentrations of indole derivatives. The measurements were performed in triplicate for each sample.

Intestine digestion, flow cytometry and cell sorting

Cells from the small intestine lamina propria were isolated as previously described[56]. Briefly, after removing payer patches and fat the small intestine was cut longitudinal open and washed in 4 changes of

Roswell Park Memorial Institute (RPMI). Next, samples were incubated under rotation for 20 min at 37 °C in RPMI containing 5 mM Ethylenediaminetetraacetic acid (EDTA), 1 mM Dithiothreitol (DTT), and 5% fetal calf serum (FCS) to remove epithelial cells. Samples were then washed 3 times in PBS and transferred to the digestion solution (RPMI containing 0.1 mg/ml Liberase TL (Roche) and 0.5 mg/ml DNase I (Roche)) and incubated for 30 min at 37 °C under rotation. The digested tissue was filtered through a 70 µm cell strainer followed by a 40/80% Percoll density gradient centrifugation. Then, the isolated cells were counted and used for flow cytometry staining.

For cell surface staining the following antibodies were used: 2.5 µg/ml Fluorescein isothiocyanate (FITC) conjugated CD45 (BD Biosciences Ref: 553079. Clone: 30-F11), 2.5 µg/ml Allophycocyanin (APC)/Fire 750 conjugated CD3 (Biolegend Ref: 100362. Clone: 145-2C11), 1.25 µg/ml Brilliant Violet™ (BV) 605 conjugated CD8a (Biolegend Ref: 100744. Clone 53-6.7), 0.625 µg/ml Alexa Fluor700 conjugated CD4 (Biolegend Ref: 100536. Clone RM4-5), 0.625 µg/ml PerCP-Cyanine 5.5 conjugated CD19 (Biolegend Ref: 115534. Clone 6D5), Zombie aqua (Bio-legend Ref: 423102), 0.625 µg/ml BV510 conjugated CD11b (Biolegend Ref: 101263. Clone M1/70), 0.625 µg/ml BV510 conjugated CD11c (Biolegend Ref: 117338. Clone N418). Intranuclear staining was performed using 2.5 µg/ml phycoerythrin (PE) conjugated T-bet (Biolegend Ref: 644810. Clone: 4B10), 0.625 µg/ml PE-Cyanine7 conjugated FoxP3 (eBioscience Ref: 25–5773. Clone: FJK-16s), 0.1 µg/ml BV-421 conjugated GATA-3 (Biolegend Ref: 653814. Clone: 16E10A23) and 0.3125 µg/ml APC conjugated ROR-γt (Invitrogen Ref: 17–6981. Clone: B2D). Samples were acquired using a flow cytometer (LSR Fortessa, Becton Dickinson) and data was analyzed using FlowJo software (Tree-Star, OR, USA). Cell doublets were excluded using forward (FSC-A vs. FSC-H) and side (SSC-A vs. SSC-W) scatter. Live CD45+ cells were sorted from the digested lamina propria of the small intestine by using a FACS Aria II (BD Biosciences).

16 S rDNA gene sequencing and analysis

16 S rDNA gene sequencing of fecal DNA samples was performed as previously described[7]. Briefly, the V3-V4 region (16 S (sense) 5′-TACG-GRAGGCAGCAG-3′ and (antisense) 5′-CTACCNGGGTATCTAAT-3′) was amplified and sequencing was done using an Illumina MiSeq platform (GenoScreen, Lille, France). Raw paired-end reads were subjected to the following process: (1) quality-filtering using the PRINSEQ-lite PERL script38 by truncating the bases from the 3′ end that did not exhibit a quality <30 based on the Phred algorithm; (2) searching and removing both forward and reverse primer sequences using CutAdapt, with no mismatches allowed in the primer sequences. Sequences for which perfect forward and reverse primers were not found were eliminated. Analysis was performed using the Qiime2 pipeline (version 2020.8.0) in R version 4.2.2[57]. Sequencing errors were corrected with Dada2[58] using custom parameters (--p-trunc-len-f 230 --p-trunc-len-r 220). Taxonomic classification of resulted ASVs was performed using Silva trained database (v138-99)[59] based on scikit-lern's naïve Bayes algorithm. Results were deep analysed with the Phyloseq package (version 1.34.0)[60] as for the analysis of taxonomic and alpha diversity. Statistical analyses were performed using rstatix[61] (version 0.7) and figures were plotted using the ggplot2 package (version 3.3.5)[62]. Principal coordinate analyses (PCoA) were carried out with Vegan package (version 2.5-7)[63] on the Bray-Curtis dissimilarity matrices constructed from the relative abundance of ASVs. Communities that emerged were verified using a PERMANOVA test with adonis2 function using 999 permutations, and the confidence interval were plotted at 95% and 97% confidence limits, using the standard deviation method.

Statistical analysis

Graphs and statistical analyses were performed using Prism software (Graphpad). Values are expressed as means ± s.e.m. Differences between values were examined using the two-tailed Mann-Whitney

test. Normal distribution was assessed by the Kolmogorov-Smirnov test. One-way analysis of variance was used to compare 3 or more independent experimental groups. The analysis was performed by Brown-Forsythe ANOVA test followed by Tukey's multiple comparison test, as appropriate. The significance of data that did not respect normality were assessed using Kruskal-Wallis, followed by post-Hoc Dunn's test. Values were considered significant at $P < 0.05$.

Reporting summary

Further information on research design is available in the Nature Portfolio Reporting Summary linked to this article.

Data availability

The authors declare that the data supporting the findings of this study are available within the paper and its supplementary information files. All the raw data generated in this study are provided in the Source Data file. Microbiota 16 s RNA data are accessible with the following link https://www.ebi.ac.uk/ena/browser/view/PRJNA996874. Raw data of the metabolites analyzed by mass spectrometry are accessible with the following link http://www.peptideatlas.org/PASS/PASS05869. Source data are provided with this paper.

References

1. Cainzos-Achirica, M. et al. Inflammatory Bowel Disease and Atherosclerotic Cardiovascular Disease: JACC Review Topic of the Week. *J. Am. Coll. Cardiol.* **76**, 2895–2905 (2020).
2. Witkowski, M., Weeks, T. L. & Hazen, S. L. Gut Microbiota and Cardiovascular Disease. *Circ. Res* **127**, 553–570 (2020).
3. Zelante, T. et al. Tryptophan catabolites from microbiota engage aryl hydrocarbon receptor and balance mucosal reactivity via interleukin-22. *Immunity* **39**, 372–385 (2013).
4. Gao, J. et al. Impact of the Gut Microbiota on Intestinal Immunity Mediated by Tryptophan Metabolism. *Front. Cell. Infect. Microbiol.* **8**, 13 (2018).
5. Agus, A., Planchais, J. & Sokol, H. Gut Microbiota Regulation of Tryptophan Metabolism in Health and Disease. *Cell Host Microbe* **23**, 716–724 (2018).
6. Hashimoto, T. et al. ACE2 links amino acid malnutrition to microbial ecology and intestinal inflammation. *Nature* **487**, 477–481 (2012).
7. Lamas, B. et al. CARD9 impacts colitis by altering gut microbiota metabolism of tryptophan into aryl hydrocarbon receptor ligands. *Nat. Med* **22**, 598–605 (2016).
8. Michaudel, C. et al. Rewiring the altered tryptophan metabolism as a novel therapeutic strategy in inflammatory bowel diseases. *Gut* **72**, 1296–1307 (2023).
9. Taleb, S. Tryptophan Dietary Impacts Gut Barrier and Metabolic Diseases. *Front. Immunol.* **10**, 2113 (2019).
10. Cole, J. E. et al. Indoleamine 2,3-dioxygenase-1 is protective in atherosclerosis and its metabolites provide new opportunities for drug development. *Proc. Natl Acad. Sci. USA* **112**, 13033–13038 (2015).
11. Polyzos, K. A. et al. Inhibition of indoleamine 2,3-dioxygenase promotes vascular inflammation and increases atherosclerosis in Apoe −/− mice. *Cardiovasc Res* **106**, 295–302 (2015).
12. Metghalchi, S. et al. Indoleamine 2,3-Dioxygenase Fine-Tunes Immune Homeostasis in Atherosclerosis and Colitis through Repression of Interleukin-10 Production. *Cell Metab.* **22**, 460–471 (2015).
13. Laurans, L. et al. Genetic deficiency of indoleamine 2,3-dioxygenase promotes gut microbiota-mediated metabolic health. *Nat. Med* **24**, 1113–1120 (2018).
14. Natividad, J. M. et al. Impaired Aryl Hydrocarbon Receptor Ligand Production by the Gut Microbiota Is a Key Factor in Metabolic Syndrome. *Cell Metab.* **28**, 737–749.e734 (2018).
15. Schroeder, B. O. & Backhed, F. Signals from the gut microbiota to distant organs in physiology and disease. *Nat. Med* **22**, 1079–1089 (2016).
16. Martin-Gallausiaux, C. et al. Butyrate Produced by Commensal Bacteria Down-Regulates Indolamine 2,3-Dioxygenase 1 (IDO-1) Expression via a Dual Mechanism in Human Intestinal Epithelial Cells. *Front. Immunol.* **9**, 2838 (2018).
17. Murphy, E. F. et al. Composition and energy harvesting capacity of the gut microbiota: relationship to diet, obesity and time in mouse models. *Gut* **59**, 1635–1642 (2010).
18. Morrison, K. E., Jasarevic, E., Howard, C. D. & Bale, T. L. It's the fiber, not the fat: significant effects of dietary challenge on the gut microbiome. *Microbiome* **8**, 15 (2020).
19. Deschênes, J., Bourdeau, V., White, J. H. & Mader, S. Regulation of GREB1 transcription by estrogen receptor alpha through a multipartite enhancer spread over 20 kb of upstream flanking sequences. *J. Biol. Chem.* **282**, 17335–17339 (2007).
20. Cani, P. D. et al. Metabolic endotoxemia initiates obesity and insulin resistance. *Diabetes* **56**, 1761–1772 (2007).
21. Chassaing, B. et al. Fecal lipocalin 2, a sensitive and broadly dynamic non-invasive biomarker for intestinal inflammation. *PLoS One* **7**, e44328 (2012).
22. Tran, H. Q., Ley, R. E., Gewirtz, A. T. & Chassaing, B. Flagellin-elicited adaptive immunity suppresses flagellated microbiota and vaccinates against chronic inflammatory diseases. *Nat. Commun.* **10**, 5650 (2019).
23. Taleb, S. Inflammation in atherosclerosis. *Arch. Cardiovasc Dis.* **109**, 708–715 (2016).
24. Mauler, M. et al. Platelet Serotonin Aggravates Myocardial Ischemia/Reperfusion Injury via Neutrophil Degranulation. *Circulation* **139**, 918–931 (2019).
25. Ghia, J. E. et al. Serotonin has a key role in pathogenesis of experimental colitis. *Gastroenterology* **137**, 1649–1660 (2009).
26. Walther, D. J. et al. Synthesis of serotonin by a second tryptophan hydroxylase isoform. *Science* **299**, 76 (2003).
27. Belkaid, Y. & Hand, T. W. Role of the microbiota in immunity and inflammation. *Cell* **157**, 121–141 (2014).
28. Murphy, E. A., Velazquez, K. T. & Herbert, K. M. Influence of high-fat diet on gut microbiota: a driving force for chronic disease risk. *Curr. Opin. Clin. Nutr. Metab. care* **18**, 515–520 (2015).
29. Villette, R. et al. Unraveling Host-Gut Microbiota Dialogue and Its Impact on Cholesterol Levels. *Front. Pharmacol.* **11**, 278 (2020).
30. Roager, H. M. & Licht, T. R. Microbial tryptophan catabolites in health and disease. *Nat. Commun.* **9**, 3294 (2018).
31. Ball, H. J., Jusof, F. F., Bakmiwewa, S. M., Hunt, N. H. & Yuasa, H. J. Tryptophan-catabolizing enzymes - party of three. *Front. Immunol.* **5**, 485 (2014).
32. Dai, X. & Zhu, B. T. Indoleamine 2,3-dioxygenase tissue distribution and cellular localization in mice: implications for its biological functions. *J. Histochem Cytochem* **58**, 17–28 (2010).
33. Chon, S. Y., Hassanain, H. H. & Gupta, S. L. Cooperative role of interferon regulatory factor 1 and p91 (STAT1) response elements in interferon-gamma-inducible expression of human indoleamine 2,3-dioxygenase gene. *J. Biol. Chem.* **271**, 17247–17252 (1996).
34. Gheorghe, C. E. et al. Focus on the essentials: tryptophan metabolism and the microbiome-gut-brain axis. *Curr. Opin. Pharm.* **48**, 137–145 (2019).
35. Mellor, A. L. & Munn, D. H. IDO expression by dendritic cells: tolerance and tryptophan catabolism. *Nat. Rev. Immunol.* **4**, 762–774 (2004).
36. Mellor, A. L., Lemos, H. & Huang, L. Indoleamine 2,3-Dioxygenase and Tolerance: Where Are We Now? *Front. Immunol.* **8**, 1360 (2017).
37. Wang, Y. et al. Kynurenine is an endothelium-derived relaxing factor produced during inflammation. *Nat. Med* **16**, 279–285 (2010).

38. Wang, Q. et al. Tryptophan-Derived 3-Hydroxyanthranilic Acid Contributes to Angiotensin II-Induced Abdominal Aortic Aneurysm Formation in Mice In Vivo. *Circulation* **136**, 2271–2283 (2017).

39. Metghalchi, S. et al. Indoleamine 2 3-dioxygenase knockout limits angiotensin II-induced aneurysm in low density lipoprotein receptor-deficient mice fed with high fat diet. *PLoS One* **13**, e0193737 (2018).

40. Melhem, N. J. et al. Endothelial Cell Indoleamine 2, 3-Dioxygenase 1 Alters Cardiac Function After Myocardial Infarction Through Kynurenine. *Circulation* **143**, 566–580 (2021).

41. Acovic, A. et al. Role of indoleamine 2,3-dioxygenase in pathology of the gastrointestinal tract. *Therap. Adv. Gastroenterol.* **11**, 1756284818815334 (2018).

42. Noonepalle, S. K. et al. Promoter Methylation Modulates Indoleamine 2,3-Dioxygenase 1 Induction by Activated T Cells in Human Breast Cancers. *Cancer Immunol. Res* **5**, 330–344 (2017).

43. Agus, A., Clément, K. & Sokol, H. Gut microbiota-derived metabolites as central regulators in metabolic disorders. *Gut* **70**, 1174–1182 (2021).

44. Schiering, C. et al. Feedback control of AHR signalling regulates intestinal immunity. *Nature* **542**, 242–245 (2017).

45. Xue, H. et al. Gut Microbially Produced Indole-3-Propionic Acid Inhibits Atherosclerosis by Promoting Reverse Cholesterol Transport and Its Deficiency Is Causally Related to Atherosclerotic Cardiovascular Disease. *Circ. Res* **131**, 404–420 (2022).

46. Bader, M. Inhibition of serotonin synthesis: A novel therapeutic paradigm. *Pharm. Ther.* **205**, 107423 (2020).

47. Sonnenberg, G. F. & Artis, D. Innate lymphoid cell interactions with microbiota: implications for intestinal health and disease. *Immunity* **37**, 601–610 (2012).

48. Berglund, E. D. et al. Glucose metabolism in vivo in four commonly used inbred mouse strains. *Diabetes* **57**, 1790–1799 (2008).

49. Barnich, N. et al. Beneficial Effects of Natural Mineral Waters on Intestinal Inflammation and the Mucosa-Associated Microbiota. *Int. J. Mol. Sci.* **22** https://doi.org/10.3390/ijms22094336 (2021).

50. Johansson, M. E. & Hansson, G. C. Preservation of mucus in histological sections, immunostaining of mucins in fixed tissue, and localization of bacteria with FISH. *Methods Mol. Biol.* **842**, 229–235 (2012).

51. Taleb, S. et al. Loss of SOCS3 expression in T cells reveals a regulatory role for interleukin-17 in atherosclerosis. *J. Exp. Med* **206**, 2067–2077 (2009).

52. Mallat, Z. et al. Induction of a regulatory T cell type 1 response reduces the development of atherosclerosis in apolipoprotein E-knockout mice. *Circulation* **108**, 1232–1237 (2003).

53. Ferchaud-Roucher, V., Pouteau, E., Piloquet, H., Zair, Y. & Krempf, M. Colonic fermentation from lactulose inhibits lipolysis in overweight subjects. *Am. J. Physiol. Endocrinol. Metab.* **289**, E716–E720 (2005).

54. Maneglier, B. et al. Simultaneous measurement of kynurenine and tryptophan in human plasma and supernatants of cultured human cells by HPLC with coulometric detection. *Clin. Chem.* **50**, 2166–2168 (2004).

55. Sellick, C. A. et al. Evaluation of extraction processes for intracellular metabolite profiling of mammalian cells: matching extraction approaches to cell type and metabolite targets. *Metabolomics* **6**, 427–438 (2010).

56. Kim, E., Tran, M., Sun, Y. & Huh, J. R. Isolation and analyses of lamina propria lymphocytes from mouse intestines. *STAR Protoc.* **3**, 101366 (2022).

57. Bolyen, E. et al. Reproducible, interactive, scalable and extensible microbiome data science using QIIME 2. *Nat. Biotechnol.* **37**, 852–857 (2019).

58. Callahan, B., Proctor, D., Relman, D., Fukuyama, J. & Holmes, S. Reproducible Research Workflow in R for the Analysis of Personalized Human Microbiome Data. *Pac. Symp. Biocomput. Pac. Symp. Biocomput.* **21**, 183–194 (2016).

59. Quast, C. et al. The SILVA ribosomal RNA gene database project: improved data processing and web-based tools. *Nucleic Acids Res* **41**, D590–D596 (2013).

60. McMurdie, P. J. & Holmes, S. phyloseq: an R package for reproducible interactive analysis and graphics of microbiome census data. *PLoS One* **8**, e61217 (2013).

61. Kassambara, A. *rstatix: Pipe-friendly framework for basic statistical tests. R package version 0.7. O*, https://rpkgs.datanovia.com/rstatix/ (2021).

62. Wickham H. Reshaping data with the reshape package. *J. Stat. Soft* 21. http://www.jstatsoft.org/v21/i12/paper (2007).

63. Oksanen, J. vegan: Community Ecology Package. R Package Version 2.4-5 (2017).

Acknowledgements

Author contributions

M.C. was involved in experimental design, conducted most experiments and analyzed data. L.L., T.R., N.M., R.A.R., E.B., N. S., M.V., and B.E. helped in some experiments. J.V. provided some technical helps. C.F. discussed estrogen effects. J.D., J-M.L., and J.C. measured Trp and Trp-derived metabolites. C.K. performed cell sorting. A.T. and H.A.O. discussed results. M.B. and H.S. performed and interpreted gut microbiota analysis, and discussed results. C.D., H.R., B.C. performed histological scoring, FISH experiments, and helped in some experiments, interpreted and discussed the results. S.T. designed the study, analyzed and interpreted the data, and wrote the manuscript.

Competing interests

The authors declare no competing interests.

Additional information

Supplementary information The online version contains supplementary material available at https://doi.org/10.1038/s41467-024-50807-x.

Correspondence and requests for materials should be addressed to Soraya Taleb.

Peer review information *Nature Communications* thanks Dominik Muller, Marit Westerterp and the other, anonymous, reviewer(s) for their contribution to the peer review of this work. A peer review file is available.

Reprints and permissions information is available at http://www.nature.com/reprints

Publisher's note Springer Nature remains neutral with regard to jurisdictional claims in published maps and institutional affiliations.